

# Structural, Morphological and Optical and Electrical Properties of $\text{Ba}_{0.4}\text{Cu}_{0.6-x}\text{La}_x\text{TiO}_3$ ( $x = 0.2, 0.4, 0.6$ ) Nanoparticles

**Dr. P. Laveena manjulatha**

Assistant Professor of Physics, HOD Department of Physics, MALD Govt Degree College, Jogulamba Gadwal, Palamuru University Telangana, India-509125.

## Abstract

The structural, morphological, optical and electrical properties of  $\text{Ba}_{0.4}\text{Cu}_{0.6-x}\text{La}_x\text{TiO}_3$  ( $x = 0.2, 0.4, 0.6$ ) nanoparticles are discussed. It begins with the preparation followed by characterization of the materials. The sample material is synthesized by hydrothermal technique and then the structure of the present sample is confirmed by diffraction pattern and compared with the respective standard JCPDS pattern. In addition, the structural parameters such as the lattice constant ( $a$ ), average crystallite size ( $D_p$ ), theoretical density ( $\rho_x$ ), porosity ( $P$ ), dislocation density ( $\rho_d$ ) and strain ( $\epsilon$ ) are evaluated. In this study, morphology is analyzed using the SEM and TEM measurements. The optical properties such as A, B-site wave numbers, force constants and optical band gap energies ( $E_{op}$ ) are studied by FTIR and UV-Visible spectrometers respectively. Electric and dielectric properties have been studied over a frequency range of 100 Hz – 1 MHz and in the temperature range from 40°C to 100°C.

**Keywords:**  $\text{Ba}_{0.4}\text{Cu}_{0.6-x}\text{La}_x\text{TiO}_3$  morphological, optical electrical properties ,FTIR and UV-Visible spectrometers.

## Introduction:

Basically the solid substances were classified into two branches based on the size of the particle or grain as bulk and nano. The scientific community mainly focused on the investigations of bulk materials for prominent applications up to 18<sup>th</sup> century. Later nanotechnology and nanoscience was extended until 19<sup>th</sup> century by revealing the significance of nanoscale towards the variation of different properties such as structural, physical, electrical, magnetic, biomedical and optical properties of the nanoparticles. In this connection the current era has been mainly concentrating on study of various nanosized substances for numerous technological applications [1] like drug delivery systems, temperature, gas, liquefied petroleum gas (LPG) and humidity sensors, photocatalysis, dielectric, ferroelectric and piezoelectric properties, nanofibers, carbon nanotubes, quantum dots and quantum wires. These can be used in the biomedical sciences for identifying the tumors in human body, surgeries etc. Meanwhile many scientists have focused their attention on the distinct properties of  $\text{BaTiO}_3$ ,  $\text{CoTiO}_3$  and  $\text{PbTiO}_3$  nanoparticles [2]. Moreover, according to the literature survey most of the ceramic substances contain the cubic perovskite structure with a general chemical formula  $\text{ABO}_3$ , where 'A' atom is located at the corner position, 'B' atom occupies the centre position of the body and oxygen atom sits at the face centre position of the face

of the cubic unit cell [3]. Normally, Barium Titanate (BT) is a promising dielectric material and exhibits very attractive and tremendous applications caused by low particle size [4]. In addition, Barium Titanate has been the most extensively investigated material by many researchers because of its excellent practical applications such as colossal magneto resistance, ferroelectric, magneto electric and electro-optic effects especially related to the industrial applications [5]. Because of intrinsic capability of perovskite structure to host dopants in different size, the BaTiO<sub>3</sub> lattice has been accommodated with large number of distinct dopants which lead to exhibit semiconducting nature. However, it has been produced by atmospheric reduction method by doping it with trivalent ions (La, Y, & Sb) at B-cationic sites [6]. The ferroelectric nature of barium titanate (BT) mainly depends upon the pressure, temperature, time of sintering, grain size, defects, and different types of doping agents. The modification of ferroelectric and dielectric properties is laid on the substitution of dopants on Ba or Ti with small concentrations [7]. Coming to the point of nanoparticles synthesis, it gives more significant results when compared with the bulk synthesis. Many researchers prepared the BT nanoparticles through various methods like hydrothermal, sol-gel, micro-emulsion, polymeric precursor and micro wave heating [8, 9]. In addition, the BT microspheres were formed via the hydrothermal method [6]. Later, the cubic structured barium copper titanate nanoparticles were prepared and investigated for structural, morphological and optical properties via the hydrothermal technique [7]. After completion of literature survey, it is concluded that no work has been carried out on La-substituted barium copper titanate nanoparticles. Hence, the authors have put in efforts on the synthesis and characterization of BCLT nanoparticles via hydrothermal method.

## Methods and methodology

### Sample Preparation:

A series of Ba<sub>0.4</sub>Cu<sub>0.6-x</sub>La<sub>x</sub>TiO<sub>3</sub> (x = 0.2, 0.4, & 0.6) nanoparticles were synthesized via hydrothermal technique. The starting raw materials of Ba(NO<sub>3</sub>)<sub>2</sub>·6H<sub>2</sub>O (99.8% purity, Sigma-Aldrich), Cu(NO<sub>3</sub>)<sub>2</sub>·2H<sub>2</sub>O (99.9 % purity, Sigma-Aldrich), LaN<sub>3</sub>O<sub>9</sub>·6H<sub>2</sub>O (99.8 % purity, Sigma-Aldrich) & TiO<sub>2</sub> (99.9 % purity, Sigma-Aldrich) were weighed according to the stoichiometric formula using a sensitive digital weighing machine. The copper nitrate and lanthanum nitrates were mixed in distilled water in 1:3 ratio. Then NaOH was added slowly to the resultant solution and found that then the p<sup>H</sup> was varying from 9 to 12. Afterwards, the total mixtures were taken into a 300 ml teflon-lined steel autoclave and furthermore, these were posted to a hot-air oven and reaction was made at 150°C for 8 hr. At the end of the experiment the autoclave was slowly cooled to room temperature. The final Ba<sub>0.4</sub>Cu<sub>0.6-x</sub>La<sub>x</sub>TiO<sub>3</sub> nanoparticles were removed from the Teflon lined autoclave and washed with acetone and distilled water till the p<sup>H</sup> became equal to 7. Later, the obtained fine powder was completely grinded and was heated for one hour.

Finally, the fine powder was characterized using characterization techniques like X-ray diffractometer (Bruker X-Ray Powder Diffraction Meter, CuK $\alpha$ ,  $\lambda$  = 0.15406 nm), High Resolution Transmission Electron Microscope (HRTEM: Model Tecnai G20, FEI, USA), Field-emission Scanning Electron Microscope (Ultra 55 FE-SEM Carl Zeiss), FT-IR spectrophotometer (IR affinity-1, Shimadzu), JASCO UV-Visible spectrophotometer (V-670 PC), LCR controller (HIOKI 3532-50) for the structural, morphological, optical, transport and electrical properties respectively.

**Results and Discussions:**

**XRD Analysis (Structural Property):**

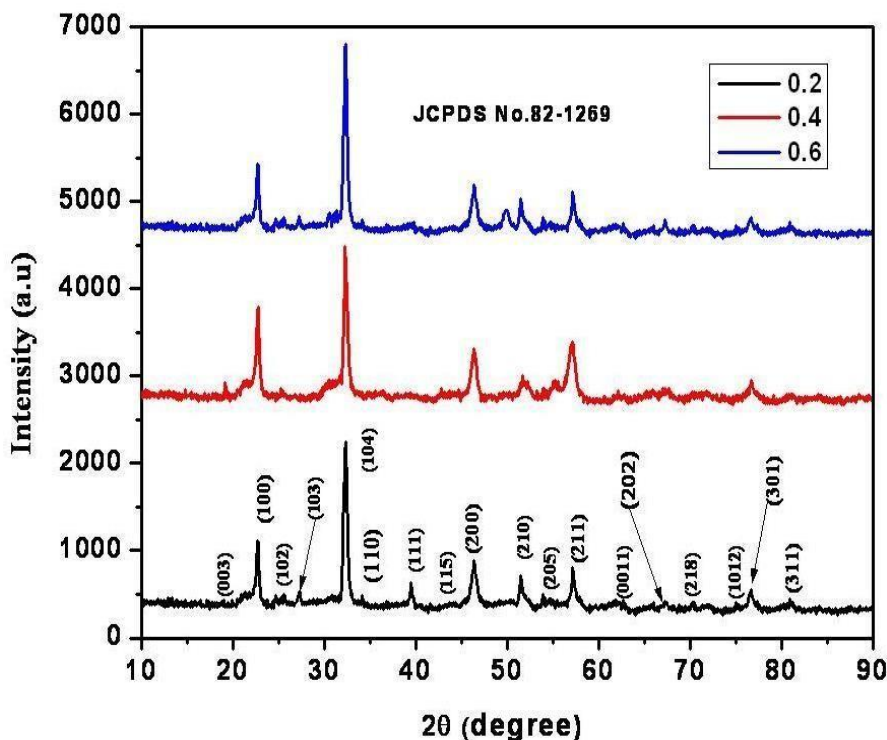


**Fig.5.1. X-Ray diffraction spectra of the BCLT nanoparticles**

Fig.5.1. was obvious that the  $x = 0.2$  to  $0.6$  contents revealed the formation of single phase tetragonal structure. The Miller indices of these tetragonal phases were indexed in the diffraction pattern. In addition, these reflection planes were in consistent with the standard JCPDS: 82-1269. All the peaks were of broad and high crystallinity in nature. However, the maximum intense peak was recorded at around  $\sim 32.142^\circ$ . Further, the average crystallite size

(D) was calculated using the Debye Scherrer method [10]. The results listed in Table.1 expressed that the ‘D’ value was noted to be changing from approximately 23 to 30 nm. Herein, the unsystematic variation of ‘D’ was attributed to the unsystematic manner of developed microstrain ( $\epsilon$ ) as a function of composition. This type of observation was also found in the literature [11-12]. Later, the lattice constants were evaluated and presented in Table.5.1. The results showed that the tetragonal lattice constants were increasing with an increase in substituent concentration. This could be due to the cationic replacement by the effect of substituent in the perovskite structure. That means, the ionic radii of cations present in BCLT material are on par with those listed according to Shannon reports [13] Viz:  $Ba^{+2}$ : 1.35 Å,  $Cu^{+2}$ : 0.73 Å, &  $La^{+3}$ : 1.032 Å, and  $Ti^{+3}$ : 0.670 Å. From these reports, it was confirmed that the La-cations of larger ionic radii will have the probability to replace the Ti-cations of smaller ionic radii [1]. Thus, there may be a possibility for the enhancement of unit cell dimensions which in turn leads to the increase of lattice constants as a function of La-content. However, it allows the increase of unit cell volume (V) as listed in Table.1. Furthermore, the X-ray density ( $d_x$ ) as well as bulk density ( $d_b$ ) were computed (Table.5.1). It can be understood from the results that both the density parameters are found to be increasing with an increase in La-content. It may be due to an enhancement of molecular weight as a function of

composition. Later, the porosity (P) was observed to be altering between 5.5 to 6.5 %. This established a fact that for the small value of pore fraction, one can expect the enhanced properties. Moreover, it is well known fact that the specific surface area (S) can be a significant parameter reflecting the better improvement of distinct material properties. In the present study, the ‘S’ value was noticed to be varying from

~14 to 30 m<sup>2</sup>/g. Moreover, we can find alternatively the average micro-strain ( $\epsilon^*$ ) and average crystallite size (D') of materials using the Williamson-Hall (W-H) plots (Fig. 5.2). In case of BCLT samples, the W-H plots were drawn between  $\beta\text{Cos}\theta$  versus  $4\text{Sin}\theta$  using linear fitting relation:  $\beta\text{Cos}\theta = 0.9\lambda/D' + \epsilon' 4\text{sin}\theta$  (i.e.  $y = c + mx$  form), herein the slope of straight line was associated to the microstrain ( $\epsilon^*$ ), and the intercept value was related to the crystallite size (D'). The obtained values of  $\epsilon'$  & D' were tabulated in Table.5.1. It was obvious from the table that both  $\epsilon'$  & D' values were in consistent with the  $\epsilon$  & D values obtained using Scherrer relations.

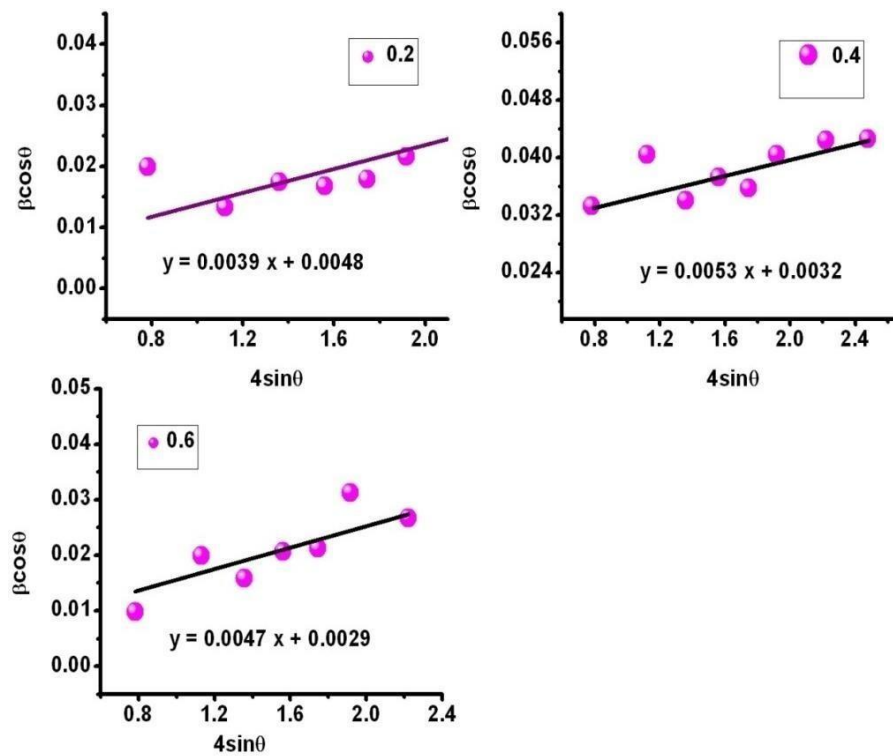


Fig.5.2. W-H plot of the BCLT nanoparticles

Table.5.1. Data on structural parameters of the BCLT nanoparticles

Parameter	0.2		0.4		0.6	
Lattice Parameter (Å)	a = b	c 3.9	a = b	c	a=b	c
	4.2		4.23	3.95	4.32	3.92
V (Å) <sup>3</sup>	74.1	59.31	75.68	61.62	80.6	80.6
D (nm)	27.24		23.13		29.87	
dx (g/c.c)	5.04		5.21		5.37	
db (g/c.c)	4.71		4.92		5.04	
P	6.5		5.5		6.1	

Microstrain ( $\epsilon$ )	0.023		0.028		0.019	
W-H strain ( $\epsilon^*$ )	0.0039		0.0053		0.047	
D' (nm)	31.71		26.42		37.22	
S ( $m^2/g$ )	17.7		29.43		13.98	

**a. FESEM Analysis (Surface Morphology Property):**

The FESEM micrographs of BCLT nanoparticles are presented in Fig.5.3. It is evident from the micrographs that all the samples reveal the well-defined and small spherical grains. In addition, these have been distributed homogeneously within the selected area of the sample. Particularly, few spots of present materials show the grains which are accumulated closely. It may be as a result of the high interactions among the nanosized grains. This kind of behavior is noted in the earlier reports [14]. Furthermore, the average grain size (G) has been evaluated with the help of linear intercept method (LIM) [15]. These are noticed to be 85 nm, 53 nm & 52 nm for  $x = 0.2, 0.4$  &  $0.6$  respectively. These results express the fact that the grain size has decreased with increase of substituent content. It may be owing to the increase of microstrain during the reaction temperature as discussed in the literature [4]. Latter, the presence of nanoparticles was confirmed using the TEM micrographs and these have been represented in Fig.5.4. It is obvious that there are large number of nanospheres like particles for  $x = 0.2$  to  $0.6$ . Herein, the morphology again includes little fiber type of elongated nanoparticles within the vicinity of nanospheres. Similar kinds of observations have been identified in the literature reported by Kumar et al. [1, 4]. From the observations of present work and the literature [1, 4], it is concluded that the presence of ferroelectric cations such as Pb & Ba and La like rare earth cations can induce the morphology of samples. Thus, these cations are capable of obtaining the change of morphology. Moreover, weak agglomeration has been detected among the nanoparticles. This may generally incur due to the interactions produced among the BCLT nanoparticles. Moreover, the particle size was found to be changing from 18 to 34 nm.

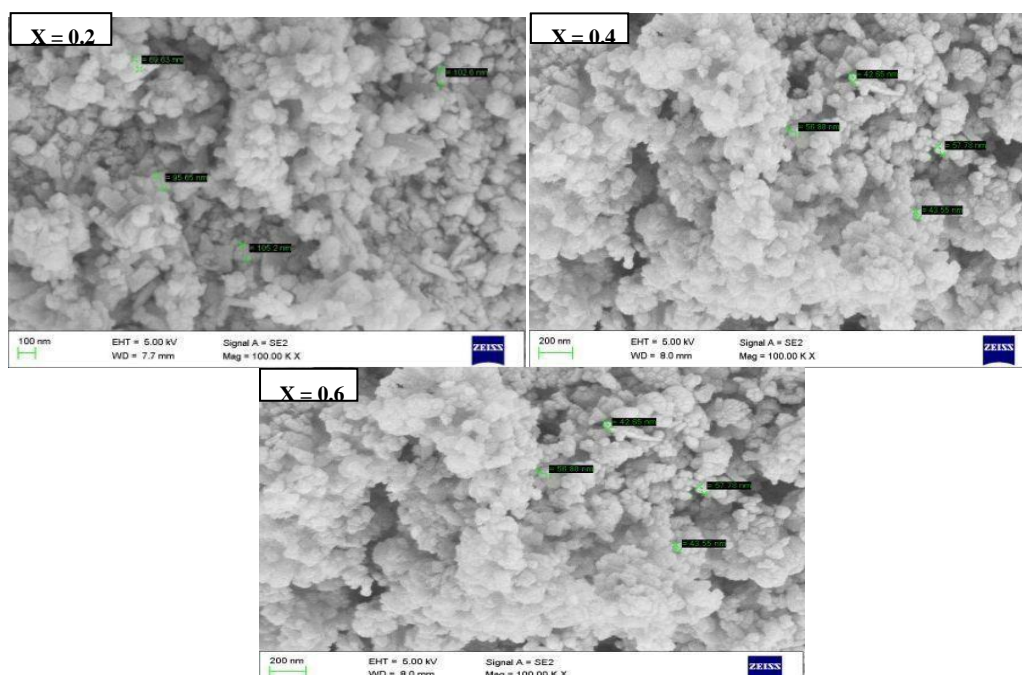


**Fig.5.3. FESEM pictures of BCLT nanoparticles**

**b. TEM Analysis (Surface Morphology Property):**

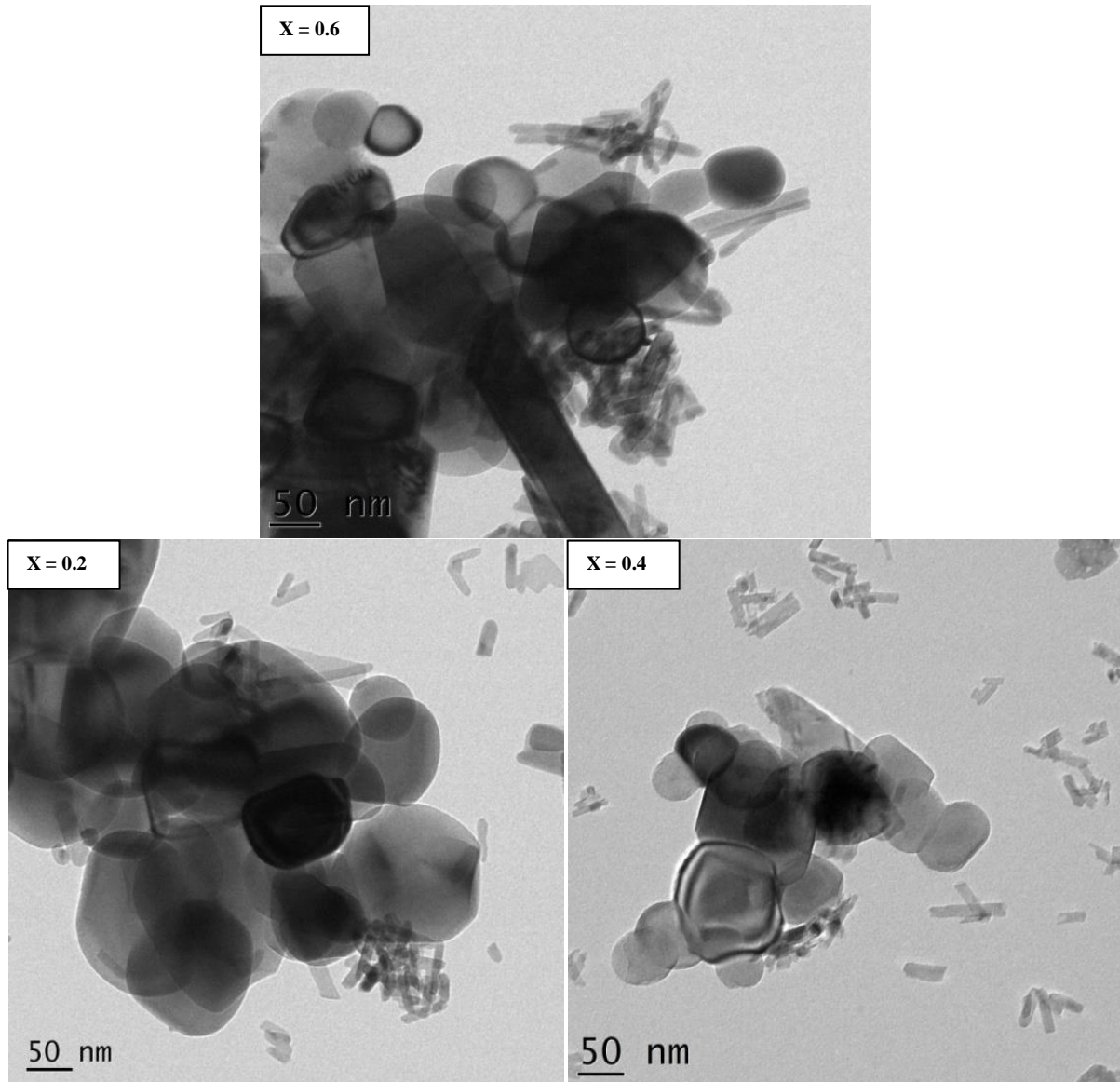


**Fig.5.4. HRTEM pictures of BCLT nanoparticles**

Further, the selected area electron diffraction (SAED) patterns of  $x = 0.4$  &  $0.6$  materials are shown in Fig.5.5. Both the SAEDs indicate the well-defined rings related to the tetragonal reflection planes with good crystallinity. Fig.5.5. provides another supportive evidence for the diffraction pattern obtained using XRD spectra.

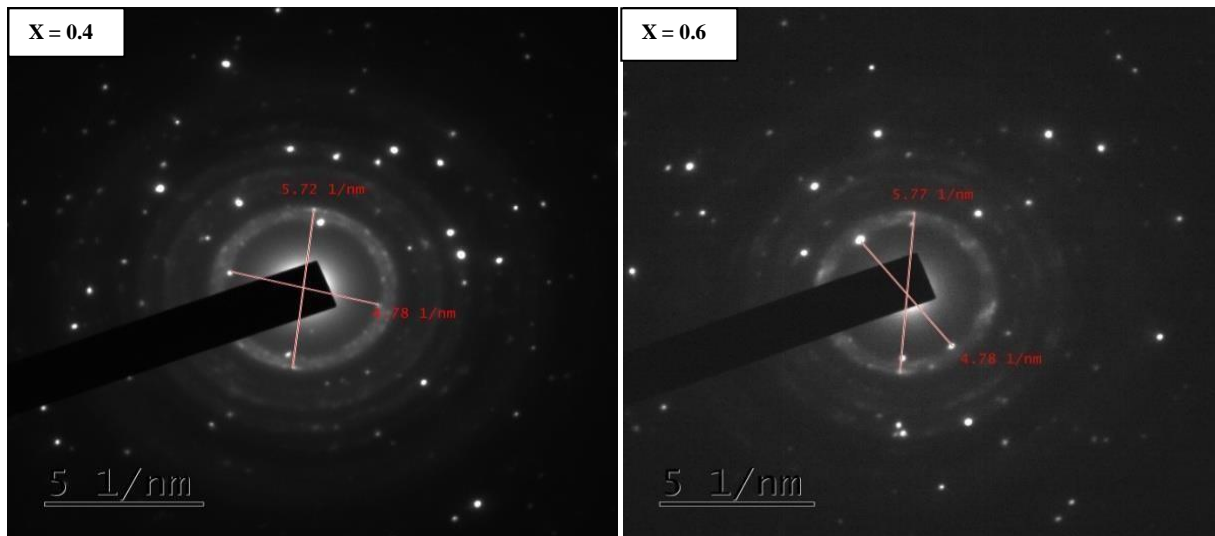


Fig.5.5. SAED pattern of BCLT nanoparticles

**a. FTIR Analysis (Optical Property):**

The FTIR spectra of BCLT nanoparticles (of ABO<sub>3</sub> perovskite form) were recorded over the frequency range of 400 to 4000 cm<sup>-1</sup> (see Fig.5.6). It was obvious from Fig.6 that the A and B-site frequencies were indicated as  $\nu_B$  and  $\nu_A$ . The frequency of A-site was noticed to be decreasing from 694.63 to 678.45 cm<sup>-1</sup> while the B-site frequency was observed to be increasing from 511.49 to 519.16 cm<sup>-1</sup>. Thus, the A and B-site formation turn in suggested the formation of ABO<sub>3</sub> perovskite structure of BCLT samples. These two sites in general will indicate the Ba-O, Cu-O, La-O and Ti-O metal oxide absorption bands. Further few absorption bands were noted at around 998.41, 1386.76, 1489.3, 1656.30, 2857.32, 2928.87, and 3429.72 cm<sup>-1</sup>. Herein, the first

three frequencies were associated to the bending vibrations of oxygen and hydrogen. These can be acquired due to the OH-absorbed the BCLT ceramic nanoparticles [1]. In the same way, the frequencies of 2857.32, and 2928.87 cm<sup>-1</sup> were correlated to the intra-molecular stretching modes which can be attributed to the various proportions of H-bonding within the BCLT perovskite structure [4]. On the other hand, the frequencies of 1656.30 and 3429.72 cm<sup>-1</sup> were interlinked sequentially to the O-H stretching vibrations as well as bending vibrations of water molecules absorbed by the BCLT nanomaterials [1].

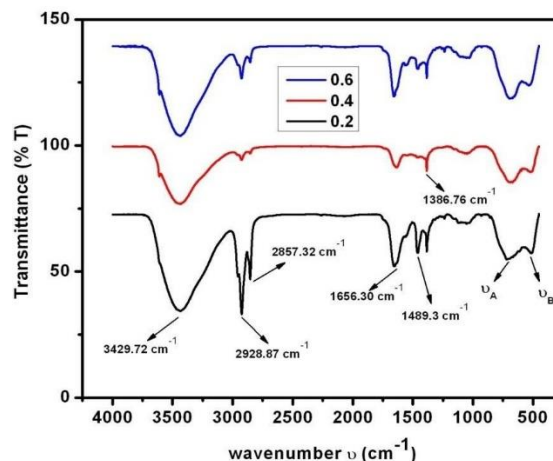
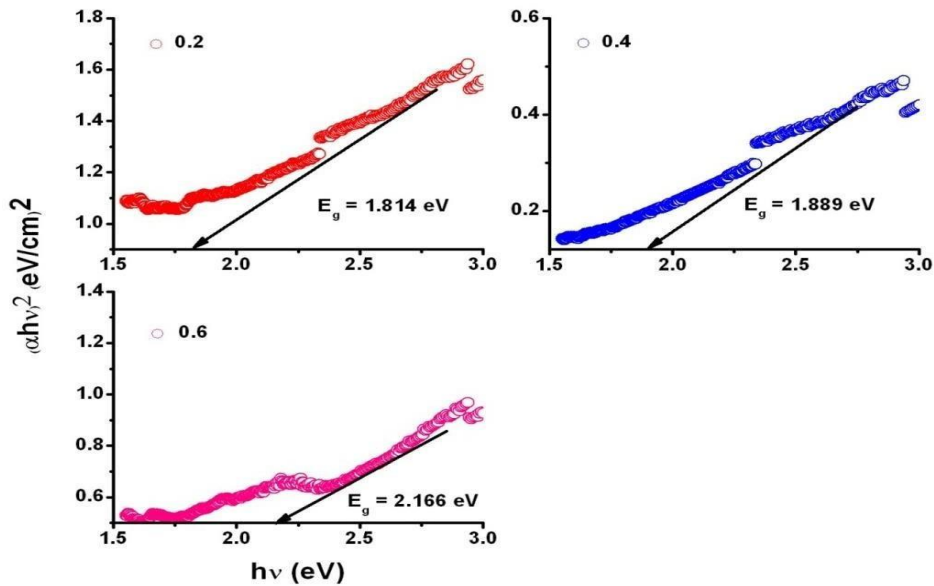


Fig.5.6. FTIR spectra of BCLT nanoparticles

**b. UV-Visible Analysis (Optical Property):**



**Fig.5.7. Optical band gap determination of BCLT nanoparticles**

In order to determine the optical band-gap ( $E_g$ ) of BCLT nanoparticles, the  $(\alpha h\nu)^n$  versus  $h\nu$  plots (where ‘ $\alpha$ ’ is absorptivity, and ‘ $h\nu$ ’ is the photon energy) were drawn by considering  $n = 2$ . Since  $n = 2$  is allowed for direct transition of charge carriers between the two energy bands [1, 4]. Hence the  $(\alpha h\nu)^n$  versus  $h\nu$  can be simply converted into the  $(\alpha h\nu)^2$  versus  $h\nu$  (as depicted in Fig.5.7). It can be obviously seen from  $(\alpha h\nu)^2$  versus  $h\nu$  plots that the  $E_g$  value was gradually increasing from 1.814 to 2.166 eV as a function of ‘ $x$ ’. The  $E_g$  value was determined by extrapolating the linear portion of the plots (Fig.5.5.) towards the photon energy axis wherein, exactly, the absorptivity identical to zero [1, 4]. From the results, one can understand that the increasing content of La predominantly induced in raising the  $E_g$  value.

**Electrical Properties:**

**Impedance analysis:**

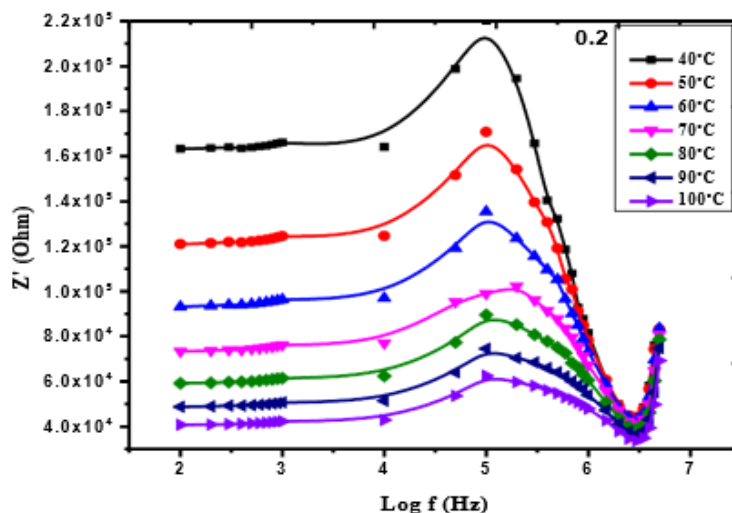


**Fig.5.8. Real part of impedance with respect to frequency at various temperatures of BCLT 0.2**

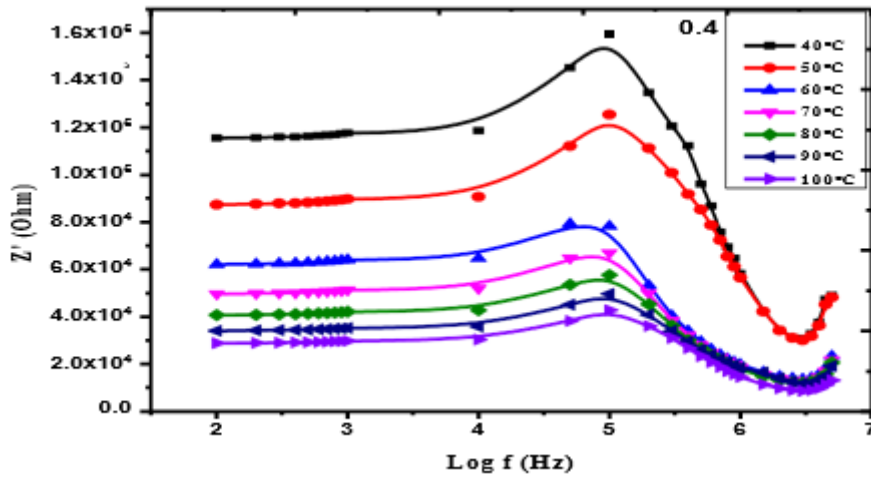


**Fig.5.9.**Real part of impedance with respect to frequency at various temperatures ofBCLT 0.4

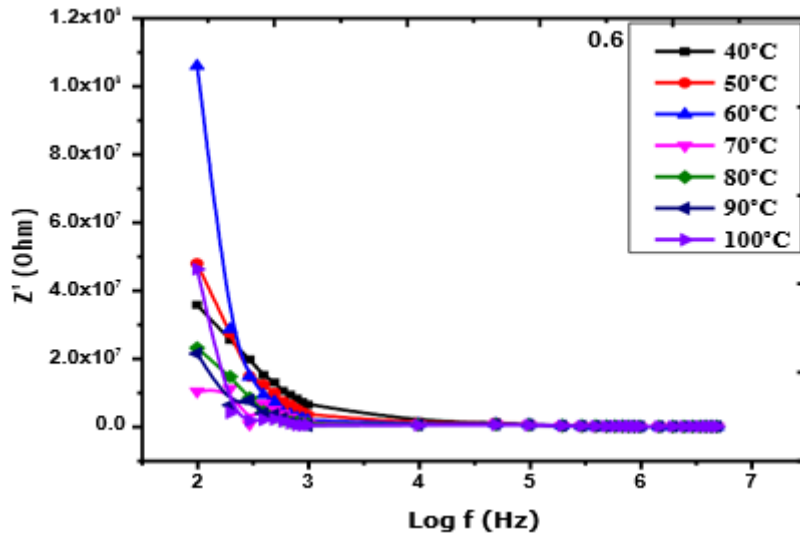


**Fig. 5.10.** Real part of impedance with respect to frequency at various temperatures ofBCLT 0.6

From the figures 5.8-5.10 the variation of real part of impedance ( $Z'$ ) of BCLT as functions of frequency (100 Hz–1MHz) at different temperatures (room temperature to 100 °C) is confirmed. It is observed from figures 5.8-5.10 that the magnitude of the  $Z'$  decreases with the increase in temperature, indicating the reduction of grain and grain boundary resistance. Higher impedance value at lower frequency region indicates the presence of space charge polarization. The  $Z'$  peak shift toward higher-frequency region with increase in temperature reveals the presence of frequency relaxation process [18-19].

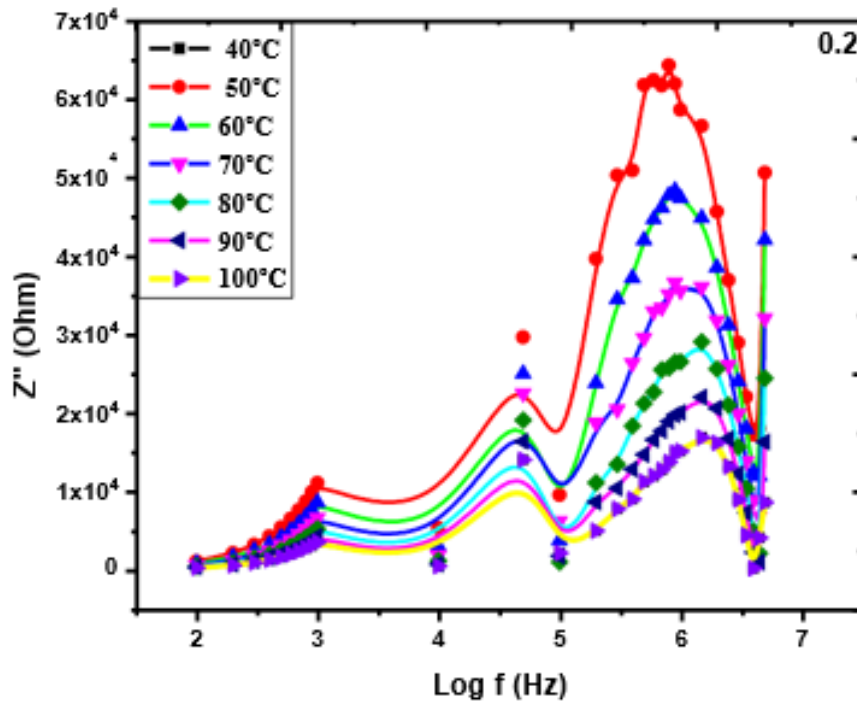


Fig.5.11. Imaginary part of impedance with respect to frequencies at various temperatures BCLT 0.2

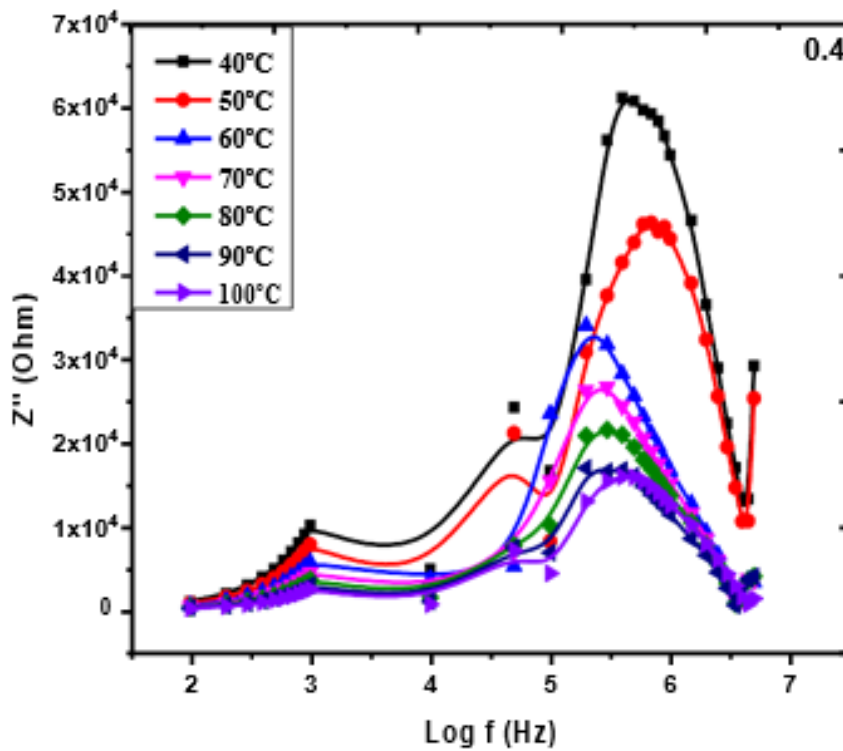
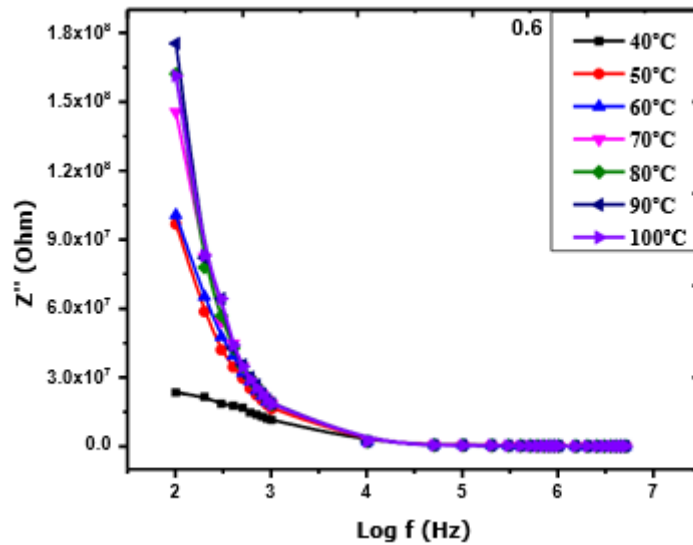


Fig.5.12. Imaginary part of impedance with respect to frequencies at various temperatures BCLT 0.4

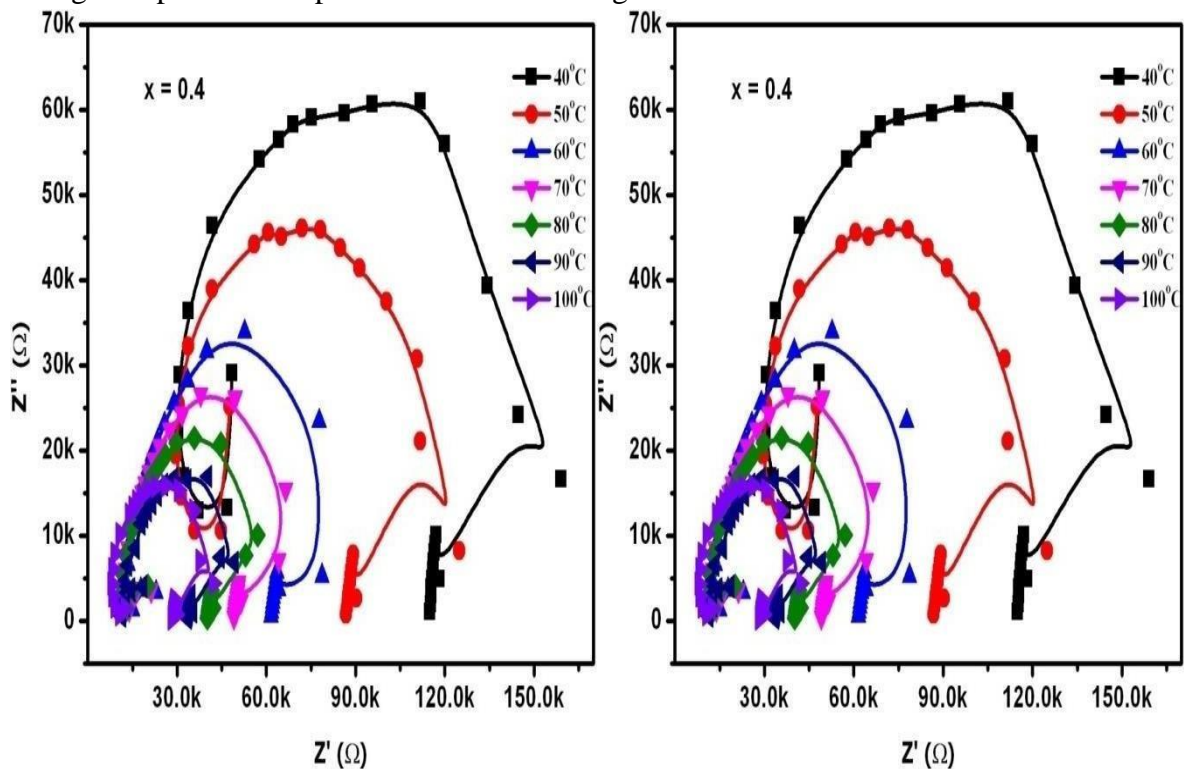


**Fig.5.13. Imaginary part of impedance with respect to frequencies at various temperatures BCLT 0.6**

It is observed from Figs. 5.11-5.13 that at any temperature  $Z''$  increases with increase in frequency, and on reaching the relaxation frequency, it starts to decrease. As temperature increases, the magnitude of  $Z''$  decreases, and the peak shifts toward higher-frequency region. The complex impedance data provides information about the relaxation process and gives frequency-dependent phenomenon associated with grain boundary regions and intrinsic properties of material in the system [18-19].

Besides, the Cole-Cole plots were drawn to understand the electrical conduction mechanism as a function of composition and temperature to mean whether it happened through grain/grain boundary contribution. Obviously, it was seen from Fig.5.14. that  $x = 0.2$  &  $0.4$  contents exhibited the complete single semi-circular arcs with considerable distortions. The complete arc formation indicated that the present BCLT materials were of semiconducting in nature. Further, the noted distortions seemed to have occurred owing to the grain size variations, defects, moisture effect, produced strain etc., as reported in the literature [4]. It was also remembered that the single arc was evolved due to the major contribution of grain rather than its boundary in the electrical conduction mechanism. Moreover, the complete relaxation strength of charge carriers was also a reason for this behavior. Clearly, it was seen that the grain or bulk resistance was found to be decreasing with increase of temperature from 40 to 100°C. Herein, the bulk resistance ( $R_g$ ) was evaluated using a technique where exactly each of the single arc intersects with the  $Z'$ -axis. Thus, the obtained results manifested that the  $R_g$  was found to be decreasing from 235 to 60 kΩ (for  $x = 0.2$  content) with temperature from 40 to 100°C. In addition, the relaxation frequency of arcs was also decreased. This incurred that at low frequencies the grain boundaries were more active while the increase of temperature reinforced the charge carriers to break the grain boundary interface and further to make motion through grain. Therefore, it was confirmed that the majority of the electrical conduction in  $x = 0.2$  content took place via the grains only. In addition, it was evident that the increase of temperature allowed increasing the electrical conductivity through conducting segments. If the centers of arcs were imagined, these were assumed to be below the real axis. Hence, it suggested that the non-Debye relaxations were predominantly observed in case of  $x = 0.2$  [4]. At 40-60°C temperature range, the origin of arcs was almost identical while it was moved to larger distance at

high temperatures. Thus, this manner indicated that the charge carriers were almost inactive at 40- 60°C temperature range which can result low electrical conduction mechanism. But, the same charges were become more active beyond the 60°C temperature which led to acquire high electrical conductivity as well. Likewise,  $x = 0.4$  content also revealed the similar trend by forming the single arcs like  $x = 0.2$ . It was observed that the bulk resistance was diminished from 185 to 47 kΩ as a function of temperature from 40 to 100°C. In comparison, this was seemed to be somewhat lesser than the bulk resistances of  $x = 0.2$ . Hence, it confirmed a fact that the electrical conductivity was increased with increase of La-content from  $x = 0.2$  to 0.4. Specifically, at 40 and 50°C temperatures, low electrical conductivity was observed while the same was high beyond 50°C. This established a fact that  $x = 0.4$  content showed significant electrical conductivity response even at low temperature (>50°C) rather than the  $x = 0.2$  (>60°C). Furthermore, the  $x = 0.6$  content performed the partial formation single semi-circular arc due to partial relaxation strength. This content showed almost insulating like nature from room temperature to 100°C. Hence, one can estimate that  $x = 0.6$  content may reveal semiconducting nature at very high temperatures. As a whole, it was clear that  $x = 0.2$  & 0.4 contents expressed the high electrical conductivity at high temperatures revealing the semiconducting behavior. Similarly,  $x = 0.6$  content still required huge temperatures to perform semiconducting nature.



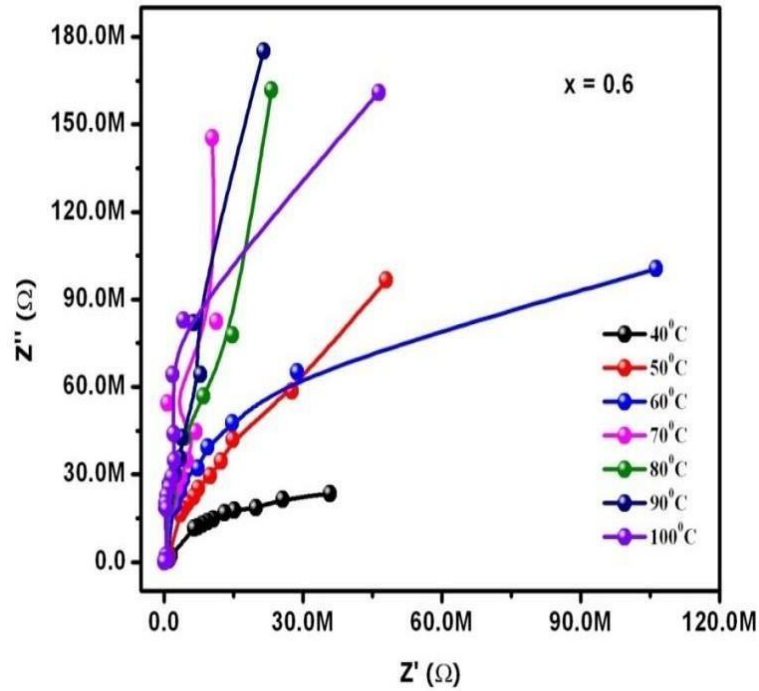


Fig.5.14.  $Z'$  versus  $Z''$  plots of BCLT as a function of La-content (0.2, 0.4, 0.6)

Dielectric response: Dielectric constant:

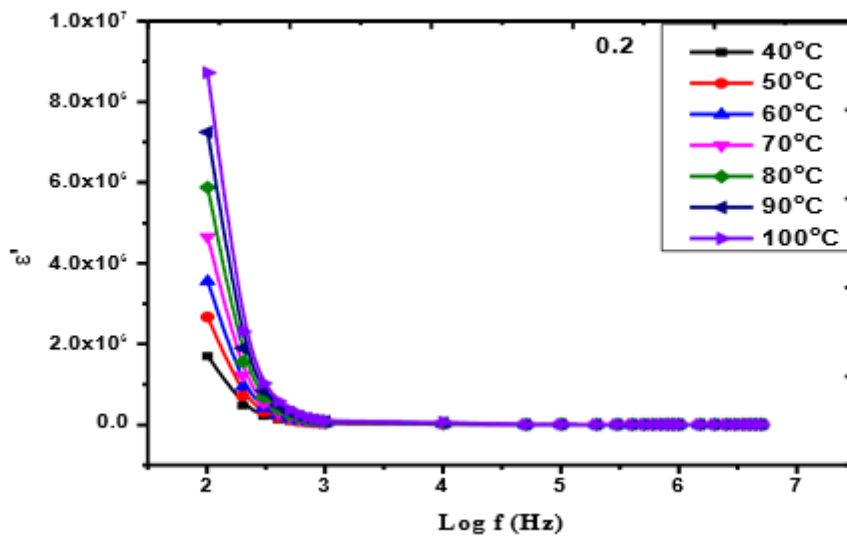


Fig.5.15. Dielectric constant as a function of frequency of BCLT 0.2

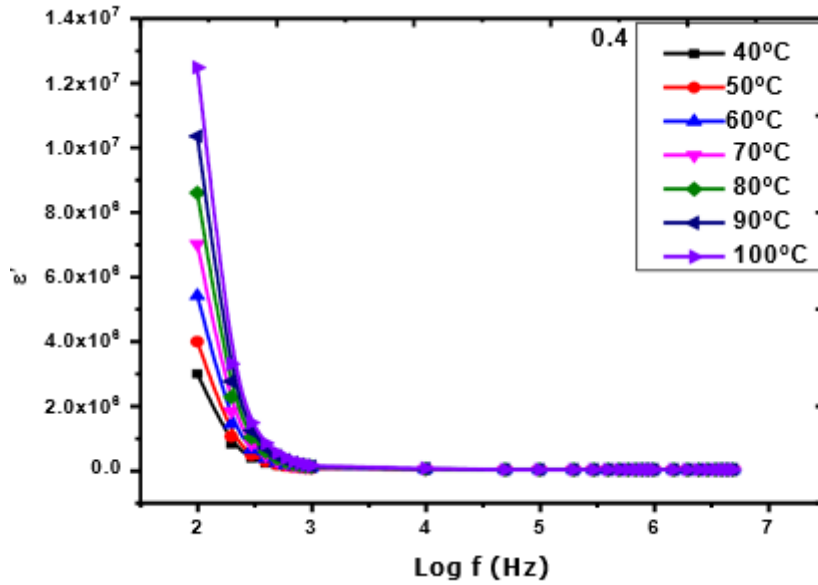


Fig.5.16. Dielectric constant as a function of frequency of BCLT 0.4

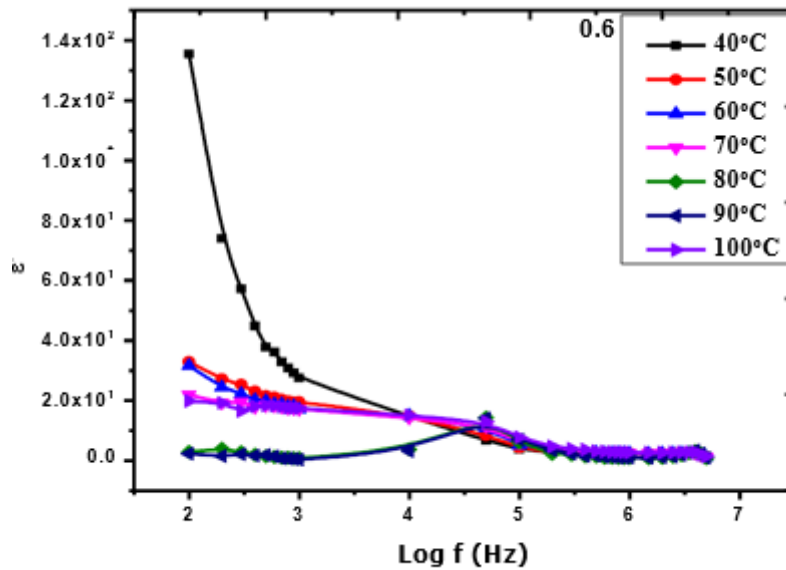
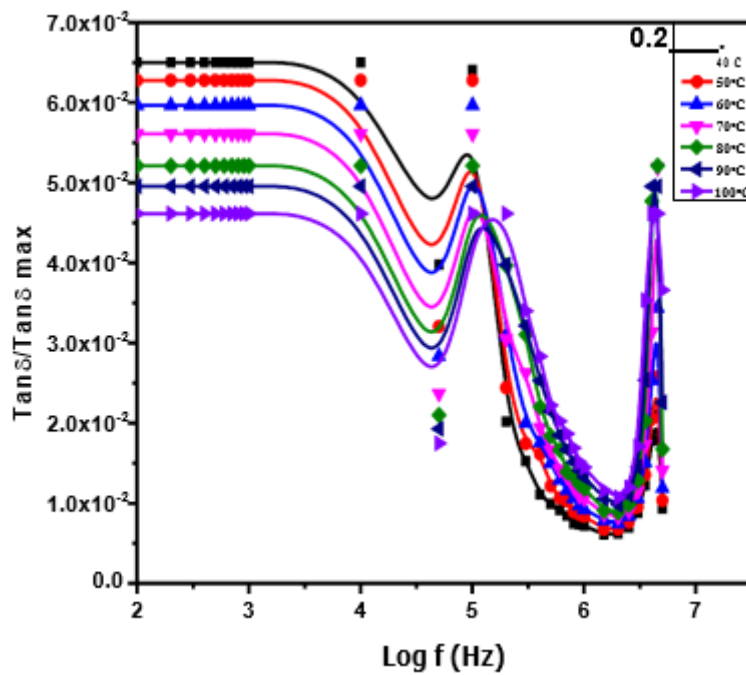


Fig.5. 17 Dielectric constant as a function of frequency of BCLT 0.6

Temperature dependence of dielectric constant ( $\epsilon'$ ) of BCLT measured in the frequency range 100 Hz to 1MHz is shown in Figs. 5.15-5.17. The decrease of the dielectric constant,  $\epsilon'$  ( $\omega$ ), is rapid at lower frequencies and showed almost frequency-independent behavior at higher- frequency region [20]. The bulk polarization of the sample results from the presence of electrodes, which do not permit transfer of the charge species into the external circuit. The behavior of the dielectric permittivity with frequency is related to the applied field, which assists electron hopping between two different sites of the sample. At higher frequency region, the charge carriers will no longer be able to rotate sufficiently rapidly, so that their oscillation will begin to lay behind this field, resulting in a decrease of dielectric permittivity,  $\epsilon'(\omega)$ . Generally, the relaxation phenomena in dielectric materials are associated with frequency dependent orientational polarization. At low-frequency region, the permanent dipoles align themselves along the

field and contribute fully to the total polarization of the dielectric. At higher-frequency region, the variation in the field is very rapid for the dipoles to align themselves, so their contribution to the polarization and, hence, to dielectric permittivity can become negligible. Therefore, the dielectric permittivity,  $\epsilon'(\omega)$  decreases with increasing frequency. The decrease of the dielectric constant  $\epsilon'$  can also be explained from interfacial polarization. The interfacial polarization arises as a result of difference in conducting phase but is interrupted at grain boundary due to lower conductivity. Generally in polycrystalline materials, the grains exhibits semiconducting, while the grain boundaries are of insulating in nature.

**5.3.5.b. Dielectric loss:**



**Fig.5.18. Dielectric loss as a function of frequency of BCLT 0.2**

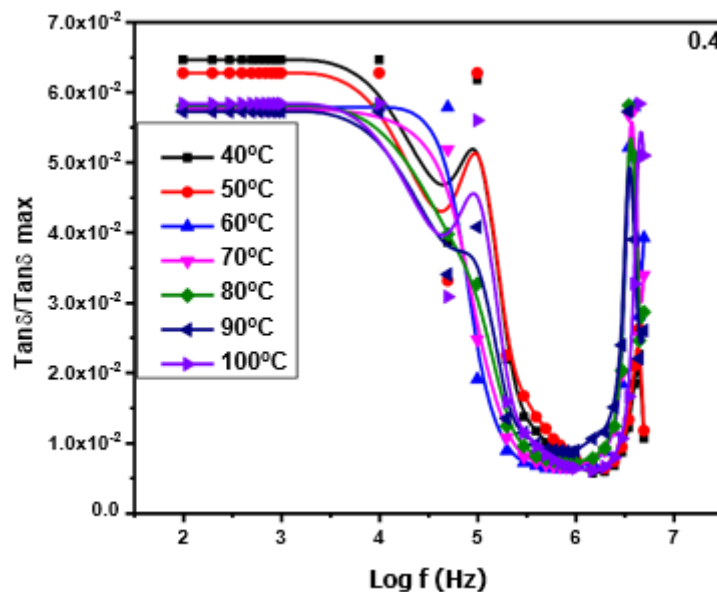


**Fig.5.19. Dielectric loss as a function of frequency of BCLT 0.4**

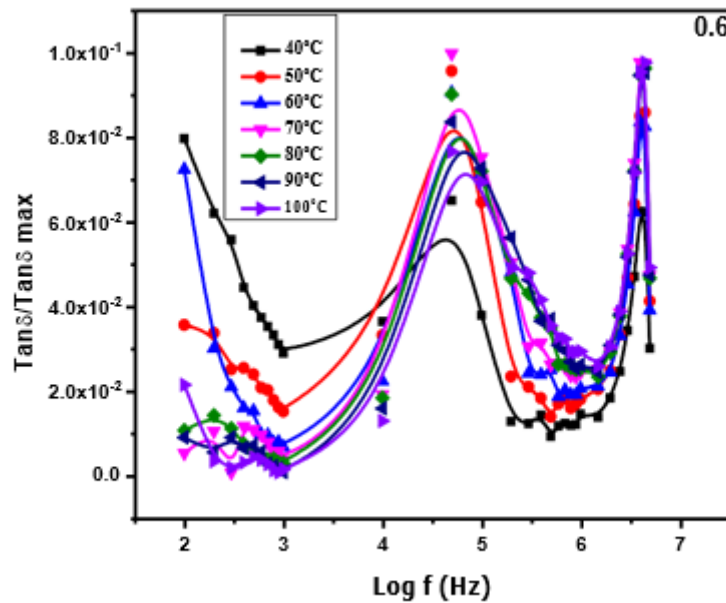


**Fig.5.20. Dielectric loss as a function of frequency of BCLT 0.6**

Temperature dependence of dielectric loss  $\tan\delta$  of BCLT measured in the frequency range 100 Hz to 1MHz is shown in Figs. 5.18-5.20. The maximum in the  $\tan\delta$  peak is shifted toward the higher-frequency region as the temperature increases, indicating a thermally activated behavior. Generally, the dielectric losses at high frequencies are much lower than those occurring at lower frequencies at specific temperature. This kind of dependence of  $\epsilon''(\omega)$  on frequency is typically associated with losses by conduction [20].

### 5.3.6. Electric Modulus Analysis:

An alternate approach to analyze electrical relaxation is electric modulus. Complex modulus formalism is a very important and convenient tool to detect the bulk phenomena properties as apparent conductivity relaxation times. It provides an insight into the electrical processes characterized by the smallest capacitance of the material. A complex electric modulus has been used to investigate the conductivity relaxation phenomena. It suppresses the effects of electrode polarization to give a clear picture of electrical property inherited in material. Modulus spectroscopy highlights bulk effects and it's complementary to impedance spectroscopy which emphasizes electrode and grain boundary effect. In the 1970 s many researches opted to study the dielectric response caused by ion relaxation using the reciprocal quantity  $M$ , known as the complex electric modulus which is defined in terms of the complex dielectric constant ( $\epsilon$ ). In order to analyze interpret experimental data; it is essential to have a model equivalent circuit that provides a realistic representation of the electrical properties. Those materials, which show a single circular arc in complex impedance plane, their electrical properties are defined by the parallel combination of grain capacitance ( $C$ ) and resistance ( $R$ ).

The electric modulus corresponds to the relaxation of the electric field in the material when the electric displacement remains constant. Therefore, the modulus represents the real dielectric relaxation process. The usefulness of the modulus representation in the analysis of relaxation

properties was demonstrated both for ionic conductors and polycrystalline materials. The complex electrical modulus can be expressed in terms of permittivity as

$$M^* = 1/\epsilon^*(\omega) = M'(\omega) + jM''(\omega) \tag{5.1}$$

$$= (\epsilon' + j\epsilon'') / (\epsilon'^2 + \epsilon''^2), \tag{5.2}$$

Where  $M'$  and  $M''$  are real and imaginary parts of complex modulus.

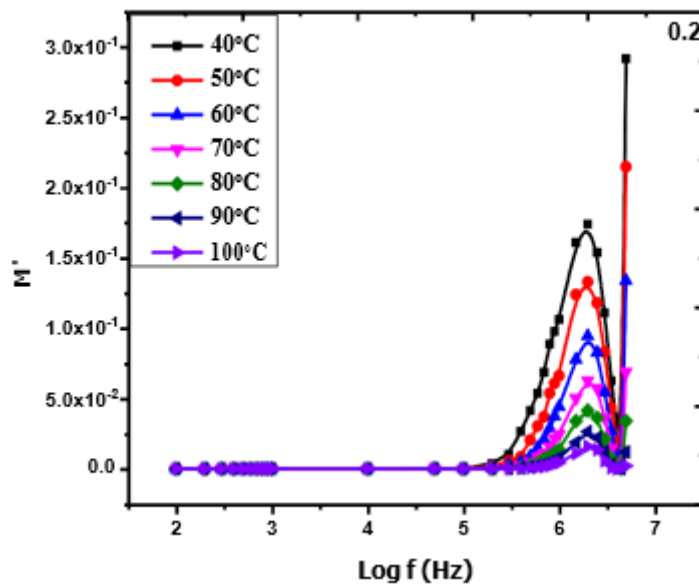


Fig.5.21. Real part of electric modulus as a function of frequency at various temperatures of BCLT 0.2

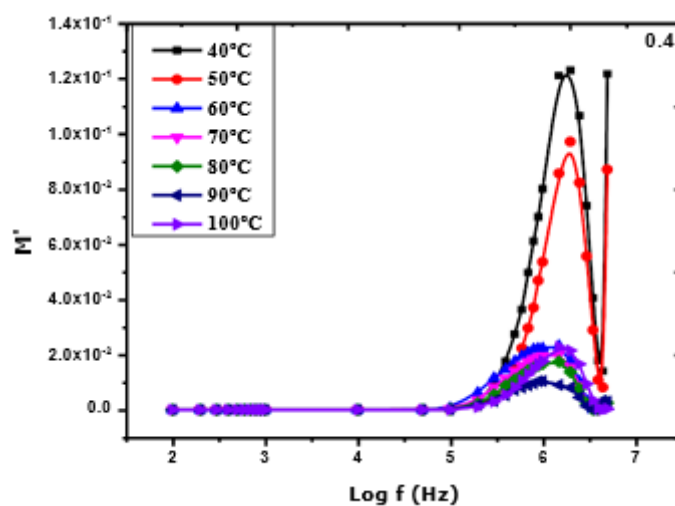


Fig.5.22. Real part of electric modulus as a function of frequency at various temperatures of BCLT 0.4

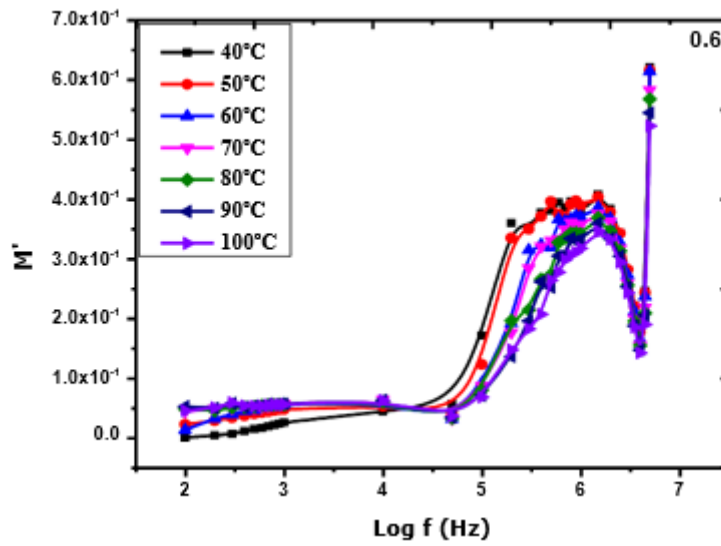


Fig.5.23. Real part of electric modulus as a function of frequency at various temperatures of BCLT 0.6

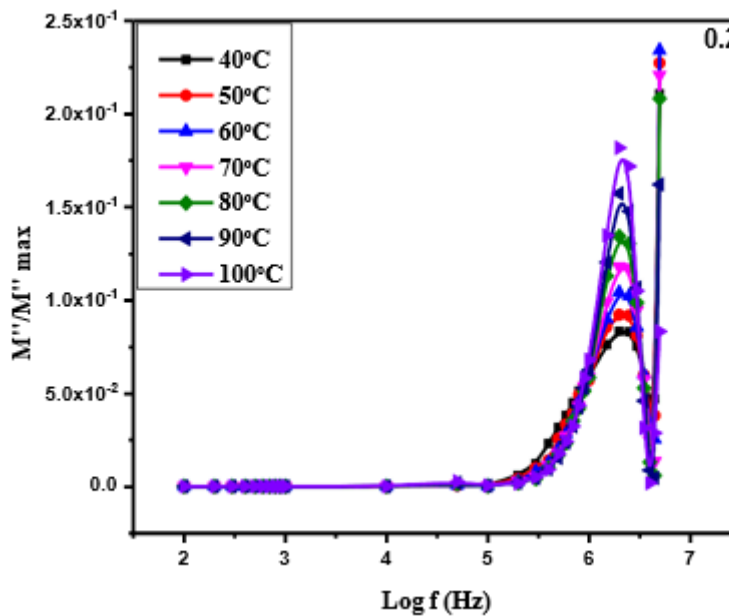


Fig.5.24. Imaginary part of electric modulus as a function of frequency at various temperatures of BCLT 0.2

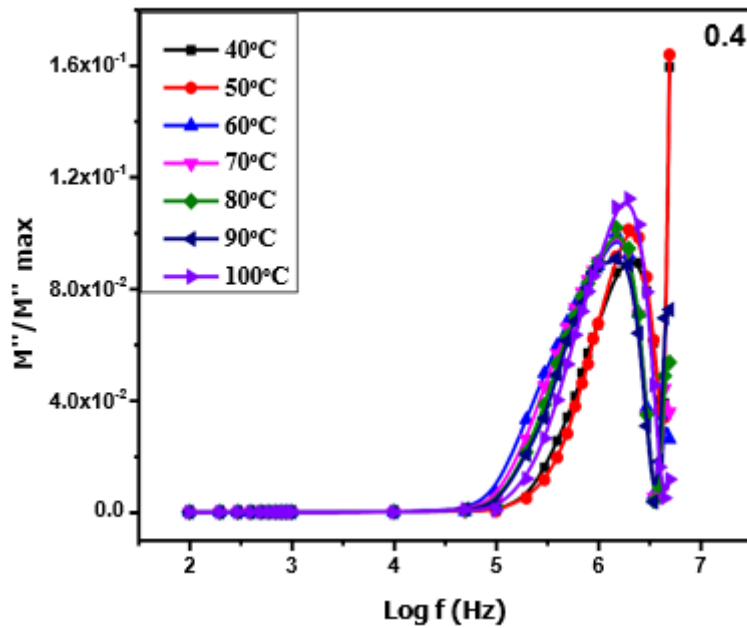


Fig.5.25. Imaginary part of electric modulus as a function of frequency at various temperatures of BCLT 0.4

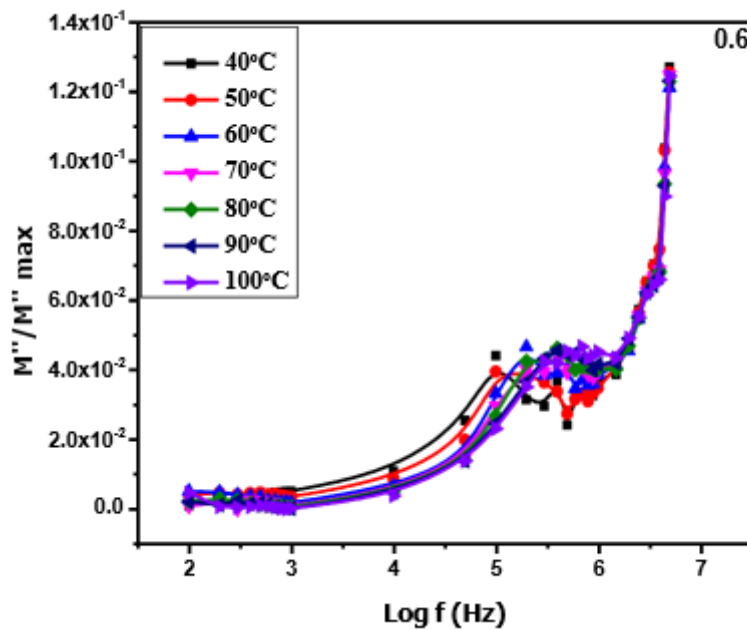


Fig.5.26. Imaginary part of electric modulus as a function of frequency at various temperatures of BCLT 0.6

The frequency and temperature dependence of real ( $M'$ ) and imaginary ( $M''$ ) parts of electrical modulus have been shown in Figs. 5.21-5.23. and 5.24-5.26. The value of  $M'$  increases with increase in frequency and almost takes nearly a constant value beyond 1MHz. At low frequency and high temperature regions  $M'$  approaches zero, which may be due to electronic and/or ionic polarization [21]. From Figs 5.24-5.26 it is evident that the imaginary part of the modulus,  $M''$  versus  $\log(f)$  for BCLT sample at various temperatures. The imaginary part of the electric modulus,  $M''$  is associated to energy loss that occurs in

the conduction process. The peak shift toward higher-frequency region with increase in temperature is clearly seen from the figure [21]. This indicates that the dielectric relaxation process is thermally activated, in which the ionic transport is by hopping. The region on the left side of the  $M''$  peak, i.e., the low-frequency region, determines the frequency range in which the mobile ions are able to hop from one site to an adjacent site. The high-frequency region represents the charge carriers being confined in potential wells that they can only move in short distance.

#### 5.4. Conclusion:

The barium copper lanthanum titanate (BCLT) nanoparticles were synthesized via hydrothermal method. The average crystallite size (D) of BCLT nanoparticles is found to be varying between 23 to 30 nm. The morphological studies showed the nanospheres like particles using the TEM. FTIR study confirmed the presence of metal oxide bonds while the UV-Visible spectral studies revealed that the  $E_g$  was increasing from 1.814 to 2.166 eV as a function of x. The Maxwell-Wagner's interfacial polarization was well understood by means of dielectric properties. In addition, the microstructure and electrical conduction mechanisms were deeply analyzed using impedance spectroscopy properties. The results pointed out that the x = 0.2 & 0.4 contents showed almost semiconducting nature even at low temperatures (60-100°C) while x = 0.6 exhibited almost insulating nature over the above mentioned range.

#### Conflicts of Interest:

The authors declare no conflict of interest. The authors declare that they have no known competing financial interest or personal relationships that could have appeared to influence the work reported in this paper.

**Acknowledgement:** Thankful to nanosensors devices lab, Vision and Electronic Sensors lab, mald department lab to carried out the work .

#### References:

1. N. Suresh Kumar, R. Padma Suvarna, and K.Chandra Babu Naidu, Sol-Gel Synthesized and Microwave Heated  $Pb_{0.8-y}La_yCo_{0.2}TiO_3$  (y = 0.2, 0.8) Nanoparticles: Structural, morphological and Dielectric properties, *Ceramics International* 44 (2018) 18189-18199
2. N. Suresh Kumar, R. Padma Suvarna and K.Chandra Babu Naidu, Phase Change and Ferroelectric Nature of Microwave Heated Lead Cobalt Titanate Nanoparticles Prepared by Sol- Gel Method, *Inter. Appl. Ceram. Tech.*, 16 (2019) 130-137.
3. Archana Shukla, R.N.P.Choudhary, A. K.Thakur, D. K. Pradha, Structural, microstructural and electrical studies of La and Cu doped  $BaTiO_3$  ceramics, *Physica B* 405 (2010) 99–106.
4. N. Suresh Kumar, R. Padma Suvarna, K.Chandra Babu Naidu, G. Ranjith Kumar, S. Ramesh, Structural and Functional Properties of Sol-Gel Synthesized and Microwave Heated  $Pb_{0.8}Co_{0.2-z}La_zTiO_3$  (z=0.05-0.2) Nanoparticles, *Ceramics International* 44 (2018) 19408-19420.
5. M.M. Vijatovic, B.D. Stojanovic, J.D. Bobic, T. Ramoska, P. Bowen, Properties of lanthanum doped  $BaTiO_3$  produced from nanopowders, *Ceramics International* 36 (2010) 1817– 1824.
6. D. Kothandan, R. Jeevan Kumar, K. Chandra Babu Naidu, Barium Titanate Microspheres by Low Temperature Hydrothermal Method: Studies on Structural, Morphological and Optical Properties, *Journal of Asian Ceramic Societies* 6 (2018)1-6
7. D. Kothandan, R. Jeevan Kumar, M. Prakash, K.Chandra Babu Naidu, Structural, Morphological and

- Optical Properties of Ba<sub>1-x</sub>Cu<sub>x</sub>TiO<sub>3</sub> (X = 0.2, 0.4, 0.6, 0.8) Nanoparticles by Hydrothermal Method, *Materials Chemistry and Physics* 215 (2018) 310–315.
8. W. Wang, L. Caon, W. Liu, Ge Su, Wenxing Zhang, Low-temperature synthesis of BaTiO<sub>3</sub> powders by the sol–gel-hydrothermal method, *Ceramics International* 39 (2013) 7127-7134.
  9. M.M. Vijatović Petrovića, J.D. Bobića, T. Ramoškab, J. Banysb, B.D. Stojanovića, Electrical properties of lanthanum doped barium titanate ceramics, *Materials Characterization* 62 (2011) 100-110.
  10. B. D. Cullity, *Elements of X-ray diffraction*, 2<sup>nd</sup> ed. (Addison-Wesley, Reading, MA, 1978)
  11. Zangina, T., Hassan, J., Azis, R.S. et al. Structural, electrical conductivity and dielectric relaxation behavior of LiHf<sub>2</sub>(PO<sub>4</sub>)<sub>3</sub> ceramic powders, *J Aust Ceram Soc* 54 (2018) 307-316
  12. Chandra Babu Naidu K., Suresh Kumar N., Ranjith Kumar G. et al., Temperature and Frequency Dependence of Complex Impedance Parameters of Microwave Sintered NiMg Ferrites, *J Aust Ceram Soc* (2018), <https://doi.org/10.1007/s41779-018-0260-x>
  13. R.D. Shannon, Revised Effective Ionic Radii and Systematic Studies of Interatomic Distances in Halides and Chalcogenides, *Acta Cryst. A* 32 (1976) 751-767.
  14. G.Aravind, M.Raghasudha, D.Ravinder, R.Vijaya Kumar, Magnetic and dielectric properties of Co doped nano crystalline Li ferrites by auto combustion method, *Journal of Magnetism and Magnetic Materials* 406 (2016)110–117
  15. K. C. B. Naidu, V. N. Reddy, T. S. Sarmash, D. Kothandan, T. Subbarao, N. S. Kumar, Structural, morphological, electrical, impedance and ferroelectric properties of BaO-ZnO- TiO<sub>2</sub> ternary system, *J Aust Ceram Soc* 55 (2019) 201-218
  16. Guo-Long Tan, Wei Li, Ferroelectricity and ferromagnetism of M-type lead hexaferrites, *J. Am. Ceram. Soc.* 98 (2015) 1812–1817
  17. Guo-Long Tan, Min Wang, Multiferroic PbFe<sub>12</sub>O<sub>19</sub>, *J. Electro. Ceram.* 26 (2011) 170–174.
  18. D. Prakash, Y. Masuda, C. Sanjeeviraja, *Solid State Ion.* 18, 31 (2012)
  19. S.K. Barik, R.N.P. Choudhary, A.K. Singh, *Adv. Mater. Lett.* 2, 419 (2011)
  20. B. Chandra Babu, V. Naresh, B. Jaya Prakash, S. Buddhudu, *Ferroelectr. Lett.* 38, 114(2011)
  21. M. Ram, S. Chakrabarti, *J. Phys. Chem. Solids* 69, 905 (2008)